

The Gutenberg-Richter Relationship vs. the Characteristic Earthquake Model: Effects of different sampling methods

Takeo Ishibe* and Kunihiko Shimazaki

Earthquake Research Institute, University of Tokyo

Abstract

The Gutenberg-Richter (G-R) relationship $\log n = a - bM$ has been used to describe regional seismicity. However, a number of studies report that the Gutenberg-Richter relationship does not hold for seismicity around late Quaternary faults or active faults during the entire seismic cycle. In this paper, we first report our study on the influences of different catalog intervals on seismicity analyses around six major strike-slip faults in southwest Japan studied by Stirling *et al.* in 1996. As a result, we find no essential differences between two observed annual occurrence rates estimated from the different catalog intervals, with the exception of the Tanna fault where the characteristic earthquake, i.e., the Kita-Izu earthquake ($M=7.3$), occurred in 1930. The results obtained after excluding all events in 1930 show much lower seismicity than that predicted by the G-R relationship. If the G-R relationship holds for one complete earthquake cycle, seismicity during a time-interval including occurrence time of the characteristic earthquake and its series of aftershocks should show much higher seismicity than that predicted by the G-R relationship, because the highest activity during a seismic cycle occurs in that period. However, the actual seismicity over 60 years including the 1930 occurrence shows, at most, activity equal to that predicted by the G-R relationship for the Tanna fault. We also discuss the bias caused by different spatial sampling methods. We propose a new method, which is applicable not only to strike-slip but also to dip-slip faults, to extract seismicity around active faults and for application to the six strike-slip fault systems using the unified Japan Meteorological Agency catalog and fault data that have been improved in recent years. The results show that the observed seismicity is lower than that predicted by the G-R relationship for all fault systems including the Yamasaki fault system, which showed higher seismicity than predicted by the previous study. These results hold even if the sampling volume is doubled.

Key words: the Characteristic Earthquake Model, the Gutenberg-Richter relationship, Late Quaternary fault, active fault

1. Introduction

The Gutenberg-Richter (G-R) relation $\log n = a - bM$, where n is the number of events with magnitudes from M to $M+dM$, and a and b are constant values, has been used to describe regional seismicity (Ishimoto and Iida, 1939; Gutenberg and Richter, 1944). On the other hand, a number of studies report that seismicity around a fault or a fault system does not satisfy the G-R relationship across the entire magnitude range for one complete earthquake cycle

(Wesnousky *et al.*, 1983; Schwartz and Coppersmith, 1984; Youngs and Coppersmith, 1985; Wesnousky, 1994; Stirling *et al.*, 1996). The magnitude-frequency distribution (MFD) around a fault shows a gap in magnitude between the largest event and other events. The largest event was named the characteristic earthquake (CE) by Schwartz and Coppersmith (1984). Figure 1 is a schematic illustration of the discrete and cumulative forms of the MFD for faults during one earthquake cycle. The CE Model has a

* e-mail: ishibe@eri.u-tokyo.ac.jp (〒113-0032 東京都文京区弥生 1-1-1)

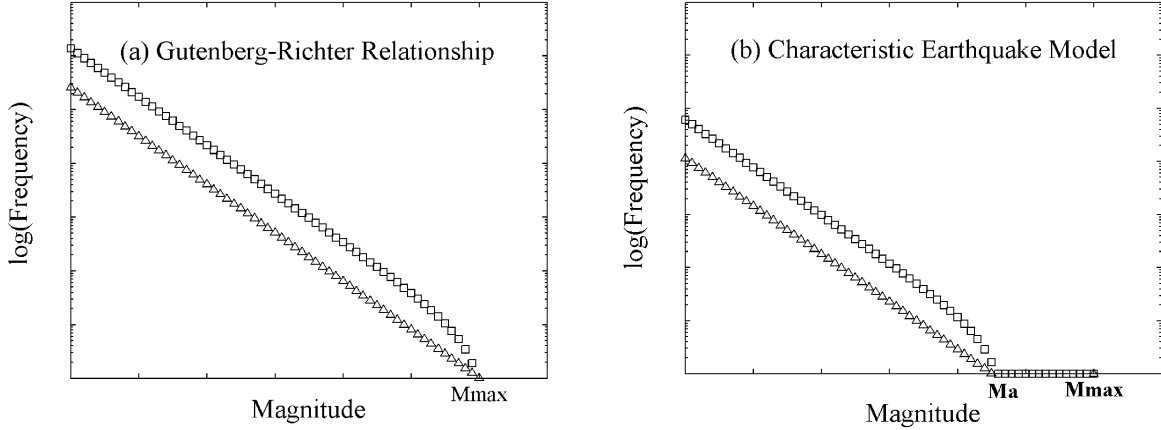


Fig. 1. Schematic illustration of discrete and cumulative forms of the MFD for faults described by (a) the Gutenberg-Richter relationship and (b) Characteristic Earthquake model during one earthquake cycle. The MFD of the G-R relationship continues to the maximum-sized magnitude, although a magnitude gap exists between maximum-sized earthquake and other events, and the size distribution of aftershocks is assumed to satisfy the Gutenberg-Richter model for the Characteristic Earthquake Model.

magnitude gap between the characteristic earthquake and the other events, although the G-R relationship assumes a continuous log-linear MFD. The number of events with magnitudes smaller than the largest event is much less than that predicted by the G-R relationship extending from the largest event.

The concept of CE may be traced back to Wallace (1970), who estimated the recurrence interval of a large earthquake based on the CE Model.

$$\tau = D / (S - C) \quad (1)$$

where τ , D , S , and C are recurrence interval, displacement caused by CE, average slip rate estimated by geological or geomorphologic data, and creep velocity, respectively. Sieh (1981)'s Uniform Earthquake Model and Wesnousky *et al.* (1983)'s Maximum Magnitude Model are other examples of the CE Model.

The simplest way to judge whether the G-R relationship or the CE Model better describes seismicity along faults or fault systems is to investigate the MFD of seismicity during one earthquake cycle. However, this is often difficult because the duration of instrumental observations is usually much shorter than the average recurrence interval of a maximum-sized earthquake, which is generally 1,000 years or longer in Japan. On the other hand, the recurrence interval of a maximum-sized earthquake can be estimated independently from geologically determined paleoearthquake histories and fault slip data. Wesnousky (1994) examined the shape of the MFD by

combining instrumental, paleoseismic, and fault data, and concluded that the CE Model holds for the southern California faults. Stirling *et al.* (1996, referred to as S96) examined 22 strike-slip faults in California, New Zealand, and southwest Japan (six strike-slip faults; the Neodani, Atotsugawa, Tanna, Yamasaki, and Atera faults, and the Median Tectonic Line fault), Turkey, and China, and concluded that the G-R relationship might hold for only four of 22 cases. Papadopoulos *et al.* (1993, 2003) concluded that the CE Model holds for the Lefkada segment of the Caphalonia transform fault in Greece.

In this study, we first examine the influences of catalog interval for the six strike-slip faults studied by S96. We use two catalog intervals: one is the Japan Meteorological Agency (JMA) catalog from 1926 to 1992, which is identical to S96, and the other is the unified JMA catalog from October 1997 to February 2005. Sampling volumes adopted by S96 vary from region to region, and are not standardized regardless of how this might affect this kind of research. Therefore, we next discuss the bias caused by different spatial sampling. We propose a method to extract seismicity around a fault or a fault system, which is not only applicable to strike-slip faults but also to dip-slip faults. Then, we apply this algorithm to the six fault systems in order to examine whether the G-R relation or the CE Model better describes seismicity during one earthquake cycle using the unified JMA catalog and fault data improved in re-

cent years.

2. Data set

In the analyses shown later, we use the unified catalog of earthquakes obtained by JMA on the basis of the recently improved seismic network. In October 1997, all instrumental records were unified by JMA, which routinely locates hypocenters. Moreover, detection capability and hypocenter accuracy have significantly improved since unification by JMA, especially in recent years after the establishment of a new seismic network called Hi-net (Obara *et al.*, 2005).

For late Quaternary active faults, we use the data set examined and compiled by the Headquarters for Earthquake Research Promotion (HERP), Ministry of Education, Culture, Sports, Science and Technology, Japan. For these fault systems, estimates were made of the locations of faults, segmentation of fault system, magnitude of characteristic earthquake, average slip rate, and average recurrence interval on the basis of the results of trenching, coring, seismic profiling, and other surveys. For active fault systems whose average slip rate is not available, we set the minimum and maximum average slip rate from the definition of degree of activity (Research Group of Active Faults, 1980, 1991); we set 1 mm/year and 10 mm/year for the minimum and maximum average slip rate, respectively, for an active fault classified as class A. When two classes are assigned into degree of activity, we use the median slip rates of the lower and higher classes as the minimum and maximum slip rates, respectively; 0.5 mm/year for the minimum and 5 mm/year for the maximum average slip rates for a fault classified as class A-B.

3. Effects of different catalog intervals

Wesnousky (1994) and S96 compared the occurrence rate of maximum-sized earthquakes to instrument observations based on the assumption that the instrumentally recorded seismicity shows the average seismicity during one earthquake cycle. However, one earthquake cycle can be divided into three intervals conceptually: mainshock-aftershock interval, inter-seismic relatively quiet interval, and pre-seismic active interval (Mogi, 1985). Therefore, the observed seismicity might depend on which stage the seismicity belongs. Moreover, seismicity might

be influenced by temporal activation or quiescence because the duration of the unified JMA catalog is less than ten years. Accordingly, we first examine the effects of catalog interval on the results for the six strike-slip faults in southwest Japan (Atotsugawa, Neodani, Atera, Tanna, and Yamasaki faults, and Median Tectonic Line fault) studied by S96. The locations of these faults and the sampling areas of earthquakes are displayed in Figure 2. S96 used the old JMA catalog from 1926 to 1992 and we use the unified JMA catalog from Oct. 1997 to Feb. 2005. The lower threshold magnitudes are set at 4.5 in their study and 1.5 in our study.

Figure 3 (a) shows the epicentral distribution of earthquakes with magnitudes equal to and above 1.5 occurring from Oct. 1997 to Feb. 2005. Figure 3 (b) illustrates the MFD for events shown in Figure 3 (a). The estimated regional b -value and its range for a 95% confidence limit are 0.84 and $+0.01$, respectively, for 26,878 shallow crustal earthquakes in southwest Japan as shown in Figure 3 (b). The old JMA catalog (1926–1992) indicates the b -value and its 95% confidence range as 0.85 and ± 0.06 , respectively, for 731 inland shallow crustal earthquakes.

The same magnitude and average recurrence interval of characteristic earthquakes as those used by S96 are assumed for comparison. The fault parameters for the six strike-slip faults used by S96 are listed in Table 1, and the earthquake magnitudes and average recurrence intervals estimated by S96 are shown in Table 2. These occurrence rates of maxi-

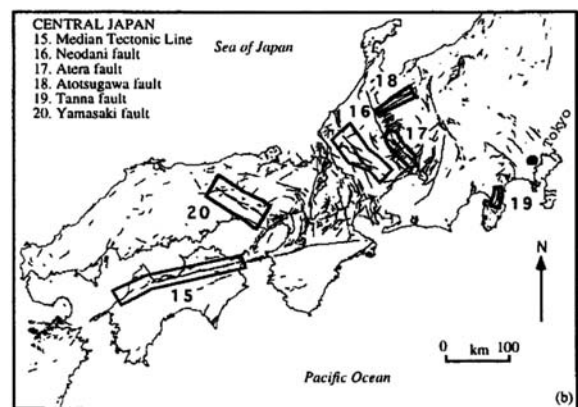


Fig. 2. Locations of six strike-slip faults studied by S96. The rectangular zone indicates areas where earthquakes are extracted for examination of seismicity around faults.

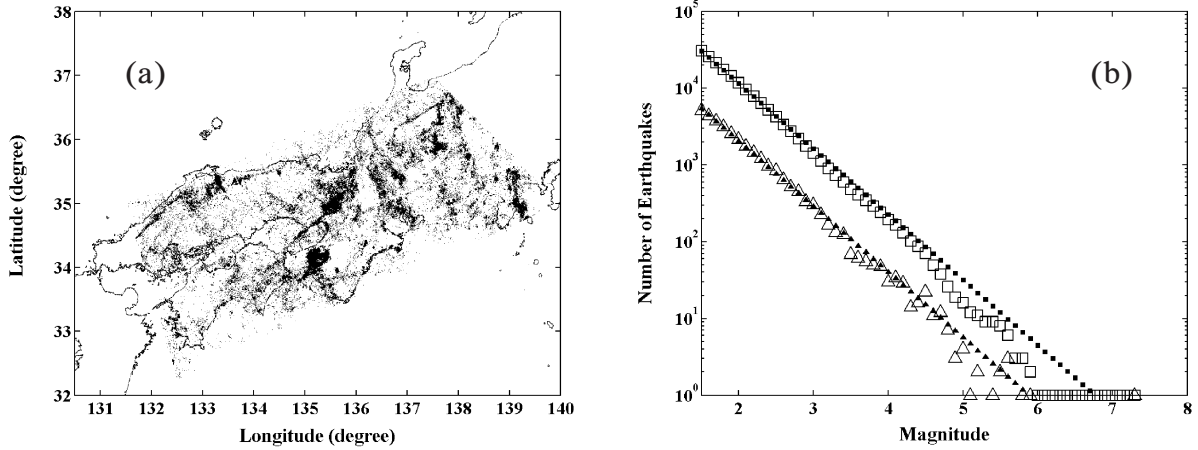


Fig. 3. (a) Epicentral distribution of shallow earthquakes with magnitudes 1.5 and above in southwest Japan. The catalog interval is from Oct. 1997 to Feb. 2005. (b) The MFD for shallow earthquakes in southwest Japan. The open squares and open triangles represent the cumulative and discrete numbers of events, respectively. The filled squares and triangles, respectively, represent the cumulative and discrete numbers of synthetic events calculated from estimated a and b -values. The b -value estimated by the maximum likelihood method for the G-R relationship and its 95% confidence range are 0.84 and 0.01, respectively.

Table 1. Geological data used by S96. These data are based on Research Group for Active Faults of Japan (1991).

FAULT	LENGTH (km)	STRIKE SLIP OFFSET (km)	SLIP RATE (mm/yr.)***	NO OF STEPS	COMPLEXITY (steps/km)
MTL	215	5	7-8(8) RL*	3-5	.014-.023
Neodani	100	3-5	1-2(2) LL**	2-3	.02-.03
Atera	60	7-10	3-5.2(5.2) LL	1-2	.017-.033
Atotsugawa	60	3	1-5 RL	2-3	.03-.05
Tanna	30	1	1-2(2) LL	2-3	.067-.1
Yamasaki	80	-	0.3-0.8 LL	0-2	0-.025

*RL : right lateral, **LL : left lateral ***the numbers within parenthesis indicate the preferred estimates

Table 2. Maximum magnitude and average recurrence interval (yrs.) obtained by S96.

Fault	Mpref	Mmin	Mmax	T1(preferred)	T2(min)	T3(min)	T4(max)	T5(max)
MTL	7.9	7.5	8.3	1188	285	326	4753	4159
Neodani	7.5	7.1	7.9	2149	667	1334	18428	9124
Atera	7.2	6.8	7.6	573	164	285	3494	2015
Atotsugawa	7.2	6.8	7.6	1195	171	855	10607	2121
Tanna	6.8	6.5	7.2	900	270	540	8944	4472
Yamasaki	7.5	7.1	7.9	22016	3036	8097	559440	209790

maximum-sized earthquake are compared to the occurrence rate of instrumentally recorded small and moderate earthquakes. The results are shown in Figure 4. In this figure, the horizontal axis represents magnitude and the vertical axis represents annual occurrence rate, i.e., inverse of the average recurrence interval. The preferred and bounding estimates of the size and the annual occurrence rate of the maximum-sized earthquakes listed in Table 2 are represented by filled and open diamonds, respectively. We

show not only the preferred estimates, but also the bounding estimates because of both uncertainties of geologically determined average slip rate and the scaling law between the magnitude of maximum-sized earthquake and the fault length (See Section 4-2 for a detailed description). A rectangular zone enclosing these open diamonds indicates uncertainties about the size and the occurrence rate of maximum-sized earthquakes. The dotted lines, representing the annual discrete number of events expected

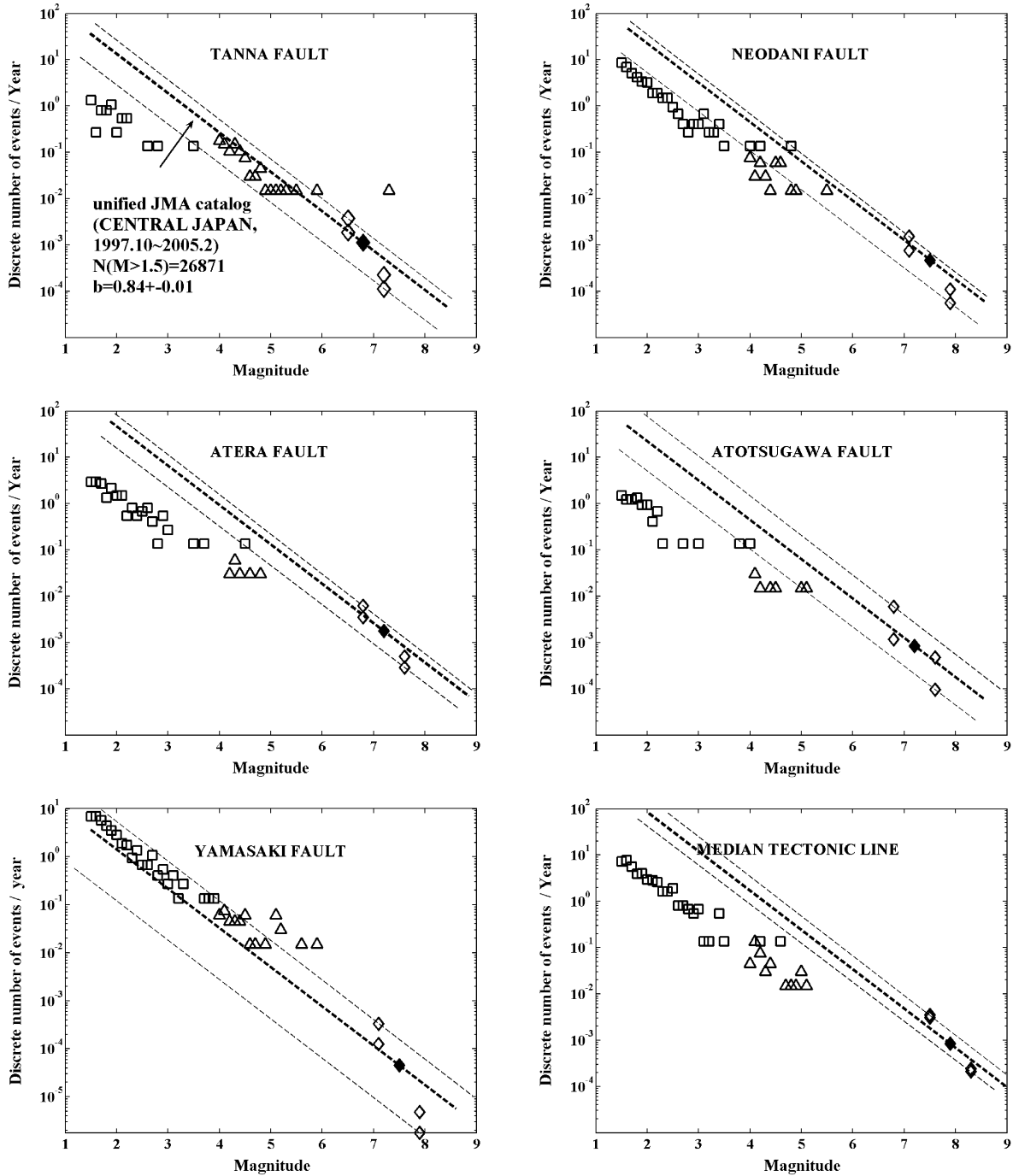


Fig. 4. Discrete number of events per year versus magnitude for six strike-slip faults in southwest Japan. The open squares represent instrumental data from the unified JMA catalog for Oct. 1997 to Feb. 2005 and the open triangles represent instrumental data from the JMA catalog for 1926 to 1992. The preferred and bounding estimates of the size and recurrence interval of maximum-sized earthquakes derived by S96 are represented by the filled and open diamonds, respectively. The dotted lines have the slope of the regional b -value of southwest Japan and indicate the annual discrete number of events predicted by the G-R relationship.

from the G-R relationship, have the slope of the regional b -value, 0.84 ± 0.01 . The bold one represents the preferred discrete number of events and the thin ones represent the minimum and maximum

of events, respectively. The open squares and open triangles represent the observed annual occurrence rate for each magnitude from the unified JMA catalog interval and the old JMA catalog interval (1926-

1992), respectively.

If the G-R relationship holds, the expected annual occurrence rates of earthquakes represented by the dotted lines should agree with the observed rates represented by the open squares and open triangles. As a result, there are no essential differences between the two observed annual occurrence rates estimated from the different catalog intervals, with the exception of the Tanna fault. In the case of the Tanna fault, the observed seismicity during the old JMA catalog interval, i.e., 1926–1992, agrees well with that predicted by the G-R relationship, although the observed seismicity for the recent time-period, i.e., Oct. 1997 to Feb. 2005, is much lower than that predicted. The Kita-Izu earthquake ($M=7.3$), occurring on 26 November, 1930, is thought to be a characteristic earthquake on this fault. Accordingly, the analysis of the old catalog is greatly influenced by this characteristic earthquake, its aftershock sequence, and preceding earthquake swarms in March and May 1930. The observed seismicity is lower than that predicted by the G-R relationship when excluding all shocks in 1930. If the G-R relationship holds for an entire earthquake cycle, seismic activity including the duration of characteristic earthquake, its aftershocks and pre-seismic swarm need to be much higher than predicted because the inter-seismic quiet interval occupies the greater part of the earthquake cycle. However, the results for the Tanna Fault indicate seismicity that is, at most, equal to that predicted by the G-R relationship, implying that the seismic activity of small and moderate magnitude events during one earthquake cycle will be much lower than predicted by the G-R relationship, and the MFD is quite close to the CE Model.

The Atotsugawa fault, the Atera fault, and the Median Tectonic Line show much lower seismicity than predicted. No significant difference between the old JMA catalog and the unified JMA catalog is found. Also, no effects of the catalog difference are found for the Neodani fault, which shows slightly lower seismicity than predicted, and the Yamasaki fault, which shows identical seismicity to that predicted by the G-R relationship.

4. Effects of spatial sampling

Sampling volume adopted by S96 is not standardized as shown in Figure 2. For example, the

distance from the Yamasaki fault to an event chosen might amount to 25 kilometers, although it might reach only about 10 kilometers for the Tanna fault. Somewhat arbitrary spatial sampling might significantly affect the results; therefore, spatial sampling should be standardized. In this study, we propose a new method to extract events around active faults, which is not only applicable to strike-slip but also to dip-slip faults. Then, we apply the method to the six fault systems. Moreover, we discuss some bias caused by differences in spatial sampling.

4-1. Spatial sampling of seismicity around active faults

A schematic illustration of how to extract seismicity around an active fault used in this study is displayed in Figure 5. The crustal volume is divided into almost cubic boxes, whose dimensions are set at 0.01 (degree) $\times 0.01$ (degree) $\times 1$ (km), and events are assigned into boxes. From geological data such as location and dip angle of a fault, cubic boxes within five kilometers (or within 10 kilometers for reference)

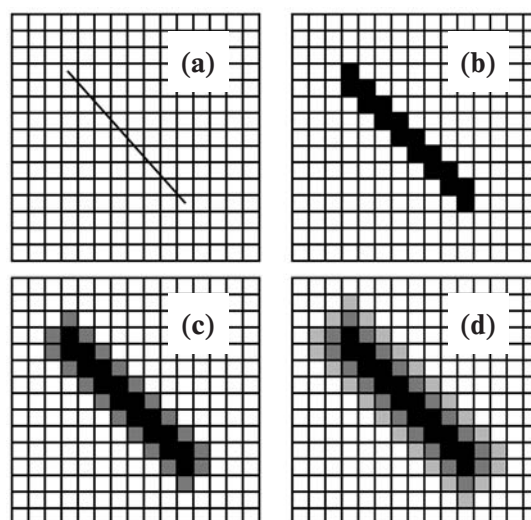


Fig. 5. Schematic illustration of sampling method in this study. Although space is divided into almost cubic boxes in the 3-D problem, this figure is represented in the 2-D problem for convenience. (a) By setting longitude and latitude of southwest and northeast corners, we extract regions that adequately cover the fault region for each fault system. (b) Extract grids that fault trace passes within it. (c) Extract grids with the distance from fault plane within one grid. (d) Extract grids with the distance from fault plane within two grids. The number of grids depends on grid interval and sampling volume.

from the fault plane are selected. Events within the selected boxes are regarded as seismicity around a fault or a fault system, and the MFD is obtained from these extracted events. Assuming that the fault extends to the whole thickness of the seismogenic layer, the fault width is estimated from both the dip angle, as was estimated by Japan Seismic Information Station (J-SHIS, 2005) and the depth of the deeper limit of microearthquakes estimated by HERP.

The number of events observed is converted into an annual occurrence rate by dividing the catalog interval. This annual occurrence rate is compared to the theoretical annual occurrence rate of events on the basis of the geologically estimated size and occurrence rate of maximum-sized earthquakes. The regional b -value of the G-R relation is estimated by the maximum likelihood method (Eq. (2)) (Utsu, 1965; Aki, 1965; Hamilton, 1967; Page, 1968; Bender, 1983; Frohlich and Davis, 1993) and the standard deviation is estimated by the method proposed by Shi and Bolt (1982) (Eq. (3)).

$$b = \frac{\log e}{E[M] - M_z} \quad (2)$$

$$\delta b = 2.3b^2 \sqrt{\frac{\sum_{i=1}^N (M_i - E[M])^2}{N(N-1)}} \quad (3)$$

where, b , $E[M]$, N , and M_z are estimated b -value, average magnitude, number of events, and threshold magnitude, respectively.

4-2. Estimation of magnitude and average recurrence interval of characteristic earthquake

HERP recognizes 24 faults or fault zones, each corresponding to a characteristic earthquake, within the six strike-slip fault zones discussed by S96. For example, the Median Tectonic Line (MTL) fault can be divided into five segmented zones, i.e., Kongo-sanchi-toen-Izumi-sanmyaku-nan'en (Kongo-Izumi), Kitan-kaikyo-Naruto-kaikyo (Kitan Naruto Kaikyo), Sanuki - sanmyaku - nan'en - Ishizuchi - sanmyaku-hokuen-tobu (Sanuki Ishizuchi Sanmyaku), Ishizuchi-sanmyaku-hokuen, and Ishizuchi-sanmyaku-hokuen-seibu-Iyonada (Ishizuchi Hokuen W-Iyonada), on the basis of the history of paleoearthquakes. The fault segmentation estimated by HERP is used in this study and is shown in Appendix B.

The magnitude and average recurrence interval of CE for 24 faults or fault zones are estimated by two different methods using geological data. One method adopts the estimates of HERP and the other follows Wesnousky's (1994) method.

HERP estimates the magnitudes of maximum-sized earthquakes from the empirical relationship proposed by Matsuda (1975) and the average recurrence interval mainly from the results of trenching surveys. Matsuda (1975) proposed the empirical relation between the magnitude of characteristic event and the fault length using 14 inland earthquakes in Japan, and obtained the relation

$$\log L = 0.6M - 2.9 \quad (4)$$

where L is fault length in km and M is magnitude of maximum-sized earthquake. For faults whose previous activity is unknown, the recurrence interval is estimated by dividing the amount of co-seismic slip estimated using the following equation (Matsuda, 1975) by the average slip rate.

$$\log D = 0.6M - 4.0, \quad (5)$$

where D is the dislocation on a fault in m accompanied by the characteristic earthquake and M is its magnitude.

The other method of estimating the maximum-sized magnitude and its average recurrence interval is identical to Wesnousky's (1994) procedure. Wesnousky (1986) indicates that the average recurrence interval of earthquakes on a fault is approximately as follows.

$$T = \frac{M_0^e}{M_0^g} \quad (6)$$

where M_0^e is the expected seismic moment for earthquakes on a fault and M_0^g is the long-term geologically assessed seismic moment rate of the fault. The seismic moment is defined as follows (for example, Aki and Richards, 1980).

$$M_0 = \mu DLW \quad (7)$$

where, M_0 , μ , L , and W are seismic moment, rigidity, fault length, and fault width, respectively. The long-term geologically assessed seismic moment rate M_0^g is derived using the average slip rate \bar{D} ,

$$M_0^g = \mu \bar{D} L W \quad (8)$$

Bounds on the seismic moment rate M_0^g are a direct function of the minimum and maximum bounds on the average slip rate \bar{D} , and the preferred estimates of M_0^g are based on the preferred average slip rate.

The seismic moment of a maximum-sized earthquake, M_0^e is obtained from the empirical relationship proposed by Wesnousky *et al.* (1983) described as follows and in Figure 6 (see Appendix A for discussion).

$$\log M_0^e = 1.94 \log L + 23.50 \quad (\text{in dyne-cm}) \quad (9)$$

Together with the preferred seismic moment of maximum-sized earthquake estimated using Wesnousky *et al.*'s (1983) formula, the following bounding estimates are adopted, which reflect the uncertainties of the scaling law.

$$\begin{aligned} M_0^e(\text{max}) &= 6 \times 10^{23} \times (L^{2.1}) \\ M_0^e(\text{pref}) &= 2 \times 10^{23} \times (L^{2.1}) \\ M_0^e(\text{min}) &= 6 \times 10^{22} \times (L^{2.1}) \end{aligned} \quad (10)$$

where $M_0^e(\text{max})$, $M_0^e(\text{pref})$, $M_0^e(\text{min})$ indicate the maximum, preferred, and minimum seismic moments of a maximum-sized earthquake. The average recurrence interval has uncertainties caused by the uncertainties regarding both the estimates of long-term geologically assessed seismic moment rate M_0^g and seismic moment of maximum-sized earthquake M_0^e . Therefore, we define the following five estimates of average recurrence interval in this study (from eq. (11) to eq. (15)).

$$T1(\text{preferred}) = M_0^e(\text{preferred}) / M_0^g(\text{preferred}) \quad (11)$$

$$T2(\text{min}) = M_0^e(\text{min}) / M_0^g(\text{max}) \quad (12)$$

$$T3(\text{min}) = M_0^e(\text{min}) / M_0^g(\text{min}) \quad (13)$$

$$T4(\text{max}) = M_0^e(\text{max}) / M_0^g(\text{min}) \quad (14)$$

$$T5(\text{max}) = M_0^e(\text{max}) / M_0^g(\text{max}) \quad (15)$$

where $M_0^e(\text{min})$, $M_0^e(\text{max})$ and $M_0^e(\text{preferred})$ are the minimum-, maximum-, and preferred-sizes of earthquakes predicted from a fault of a given length, determined from equation (10), respectively. $M_0^g(\text{min})$, $M_0^g(\text{max})$ and $M_0^g(\text{preferred})$ are the minimum-, maximum-, and preferred moment accumulation rates determined by the minimum and, maximum bounds, and preferred values for average slip rate, respectively. $T(\text{min})$, $T(\text{max})$, and $T(\text{preferred})$ are the estimated recurrence interval of the minimum-, maximum-, and preferred-sized earthquakes on each fault, respectively.

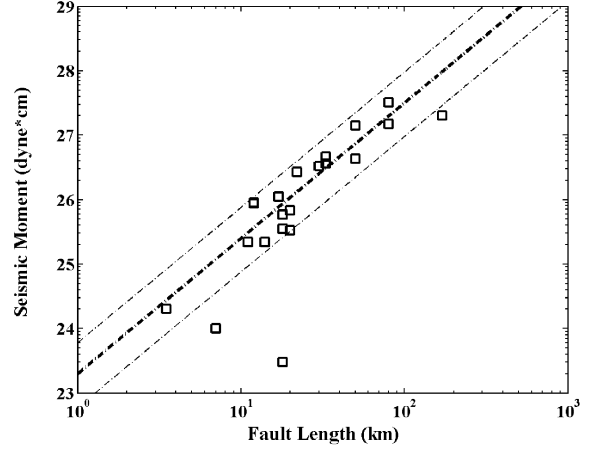


Fig. 6. Seismic moment versus rupture length for large intraplate earthquakes in Japan (from Wesnousky *et al.*, 1983).

The magnitude of a maximum-sized earthquake is obtained by converting the seismic moment of a maximum-sized earthquake into moment magnitude using the definition of moment magnitude (eq. (16); Hanks and Kanamori, 1979).

$$M_w = \frac{(\log M_0 - 16.1)}{1.5} \quad (16)$$

where M_w and M_0 are moment magnitude and seismic moment, respectively. No conversion from M_w to M_{JMA} was made as it was by S96.

If the G-R relationship holds for seismicity around a single fault or a fault system during one earthquake cycle, the occurrence rate expected by the G-R relationship will agree with that of observed seismicity around the late Quaternary active faults. Therefore, we compare the number of observed events to the number of expected events from the G-R relationship to investigate the shape of the MFD of seismicity along the fault during one earthquake cycle.

5. Result

The results for the 24 segmented zones of the six strike-slip fault systems are displayed in Figure 7. The symbols are the same as in Figure 4 except for the filled triangles representing annual occurrence rate and magnitude of maximum-sized earthquake estimated by HERP if they are available. Figure 8 is a histogram of the frequency ratio, which is defined as the ratio of the number of observed events to that

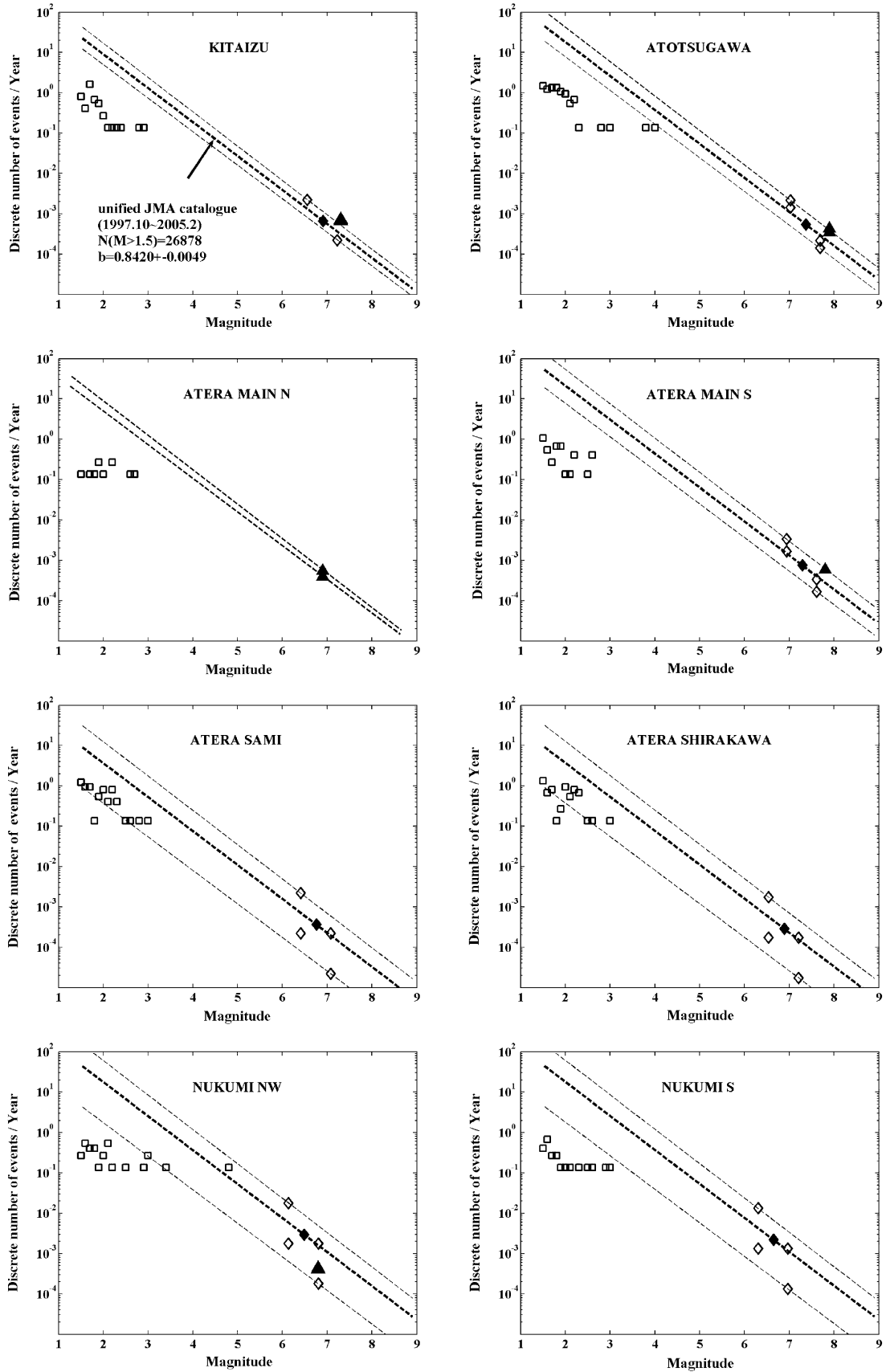


Fig. 7. The results for six strike-slip fault systems. The symbols are the same as in Figure 5 with the exception of the filled triangle that represents annual occurrence rate of maximum-sized earthquake estimated by HERP if they are available.

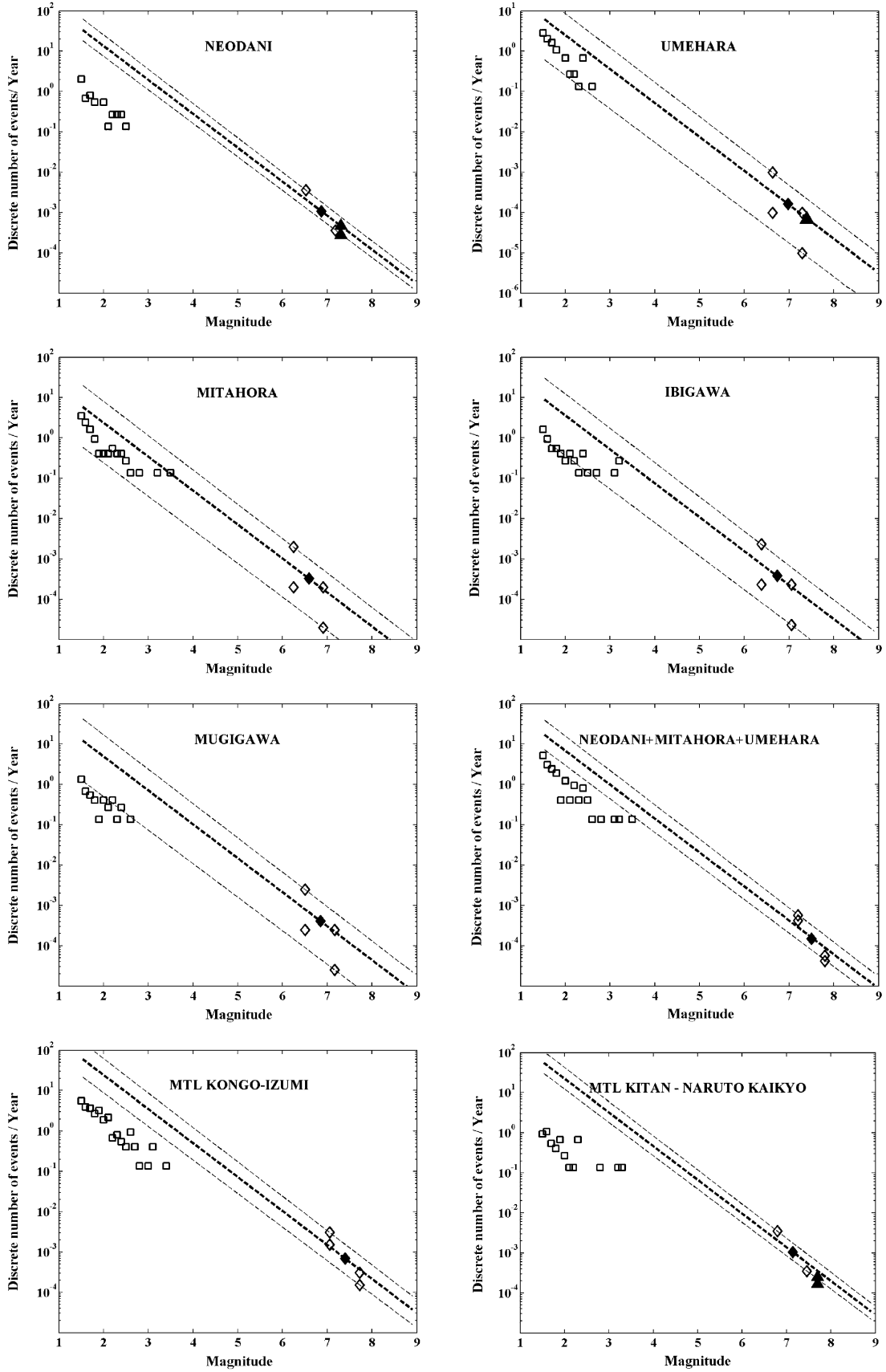


Fig. 7. (continue)

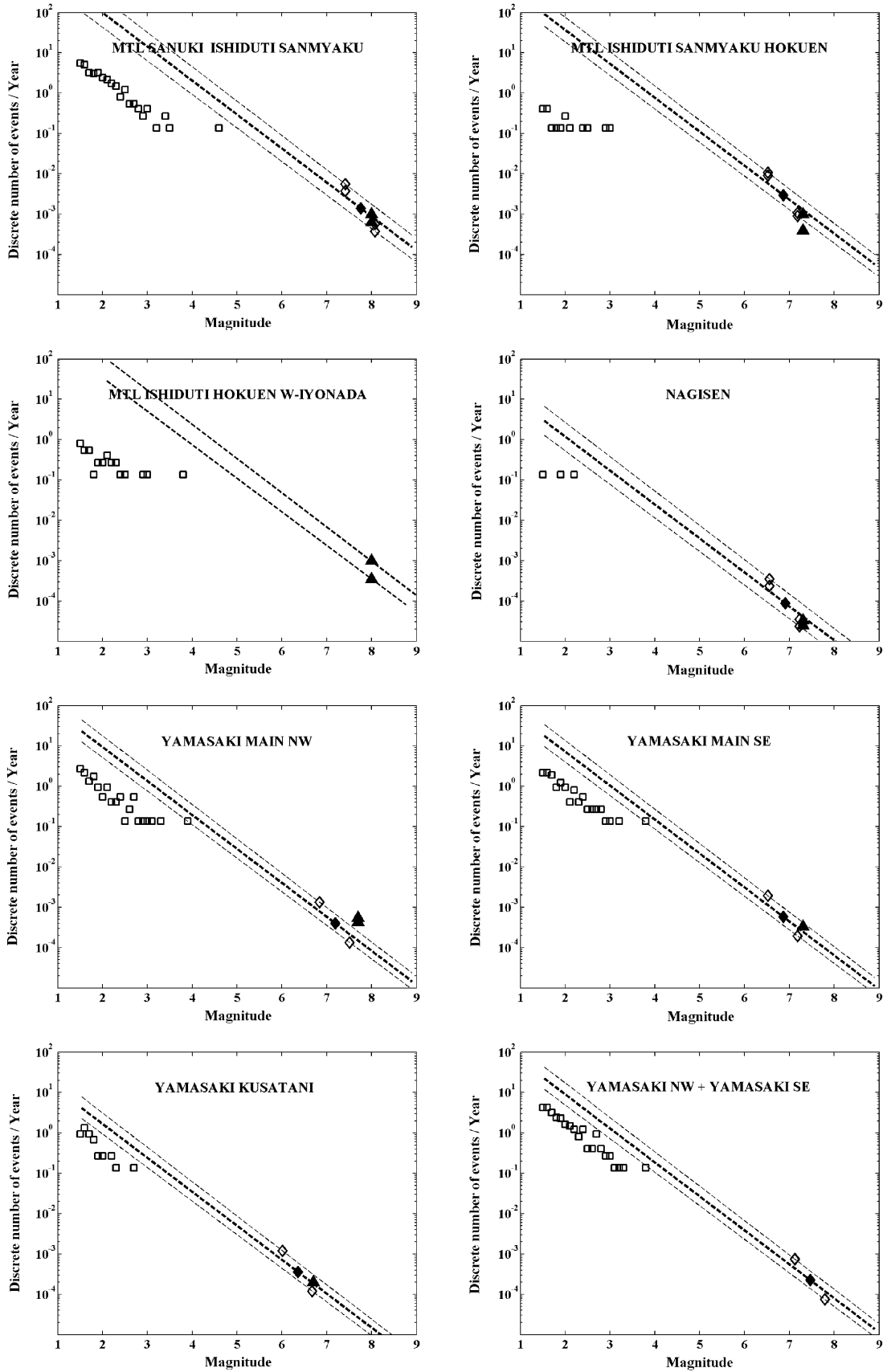


Fig. 7. (continue)

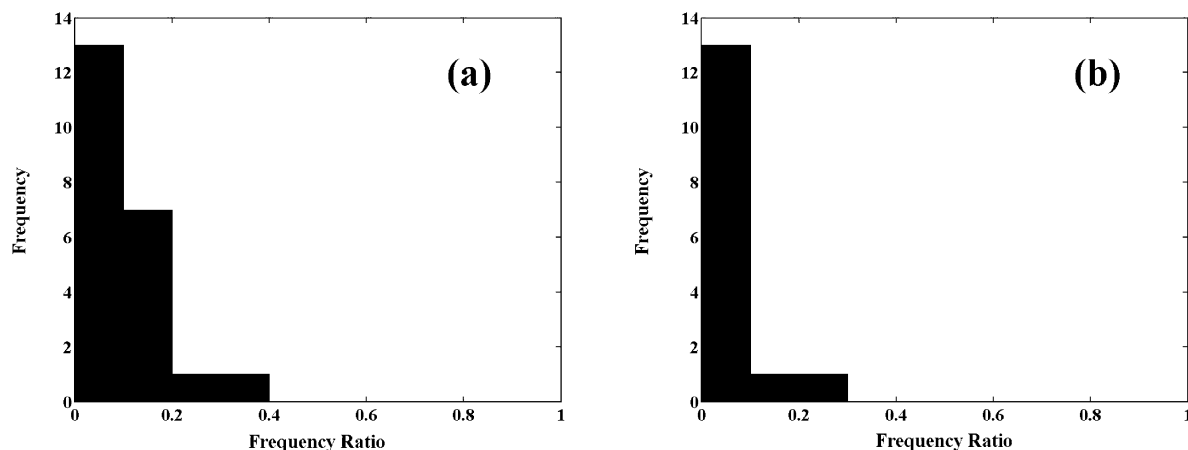


Fig. 8. Histogram of frequency ratios defined by number of observed events divided by number of events predicted by the preferred G-R relationship with magnitudes above 1.5. The number of expected events is extrapolated from the occurrence rate of maximum-sized earthquake estimated by a method identical to Wesnousky (1994) for (a), and extrapolated from the occurrence rate of maximum-sized earthquake estimated by HERP for (b).

predicted by the G-R relationship. As a result, the number of observed events is significantly less than the number of events predicted by the G-R relationship for almost all faults or fault systems, and the frequency ratio is about 0.10 on average (Figure 8 (a)). This result is obtained for the case of seismicity within 5 km from the fault, and it increases to 0.20 for seismicity within 10 km.

The seismic activity of the Yamasaki fault is much higher than predicted by the G-R relationship in S96's study. However, the preferred average recurrence interval of a maximum-sized earthquake was 22,016 years in their study, and their result is probably biased by this extremely long estimated average recurrence interval. Paleoseismicity on the Yamasaki fault has been revealed in recent years, and the fault can be divided into two segments: the northwest part and the southeast part. The estimated average recurrence intervals estimated by the Wesnousky's (1994) method are 2,506 for the northwest part and 1,751 years for the southeast part. Besides, the estimated average recurrence intervals estimated by HERP are 1,800–2,300 for the northwest and about 3,000 years for the southeast parts. The results from up-dated fault data indicate lower seismicity than predicted by the G-R relationship. Average recurrence interval for faults where only two paleoearthquakes are known such as the Umehara and Mitahora fault systems, has large uncertainties regarding average recurrence interval; therefore, it

is difficult to judge whether the G-R relationship or the CE model better describes the MFD for these faults.

6. Discussion

6-1. Short instrumental records compared to the average recurrence interval

It is impossible to examine the shape of the MFD for the entire earthquake cycle using only instrumental data. Therefore, we need to compare the occurrence rate of maximum-sized earthquakes determined by geological data and that of small and moderate earthquakes observed with instruments. S96 discussed the possibility that the G-R relationship might hold during one earthquake cycle caused by the shortness of the catalog interval compared to the average recurrence interval. They calculated the ratio of the number of observed events with magnitude 4.0 to that of events predicted by the G-R relationship, and the ratio exceeds one for only four of 22 faults. From the Monte-Carlo simulation, they indicate that events of more than ten times that predicted by the G-R relationship are necessary during a time-period less than 20% of one earthquake cycle to satisfy the G-R relationship. Accordingly, we cannot deny the possibility that the G-R relationship holds for the entire earthquake cycle if 20% of faults or fault systems indicate seismicity as high as ten times that predicted by the G-R relationship. However, the number of observed events is significantly less than

expected for almost all faults or fault systems. As pointed out earlier, the analysis of the Kita-Izu Fault System (Tanna fault) during the time-period from 1926 to 1992, including the occurrence times of the 1930 Kita-Izu earthquake, its aftershocks, and pre-seismic swarms indicates seismicity that is at most equal to the number of events in accord with the G-R relationship.

6-2. Sampling volume

In this study, we extracted events within five kilometers from the fault plane, and we also extracted events within 10 kilometers for reference. Both cases lead to the same conclusion, and it appears to be robust. Our five-kilometer sampling seems to be sufficient because Itaba *et al.* (2004) indicate that the existence of a fault has an influence on seismicity within two to four kilometers from the fault, regardless of fault type using the unified JMA catalog. Our sampling volume is also supported by the distribution of aftershocks of a large shallow crustal event in inland Japan. One typical example would be the extent of aftershocks of the Western Tottori Earthquake ($M=7.3$) on 6 October, 2000. Because the fault plane of this earthquake is found to be almost vertical, the spatial extent of the epicentral distribution of aftershocks would show the proper range of extraction. Figure 9 shows the epicentral distribution of foreshocks, mainshock, and aftershocks occurring from October 2000 to February 2005. This figure shows that the spatial extent of aftershocks is, at most, ten kilometers in width. Assuming that the fault plane is at the center of the aftershock region, most aftershocks lie within five kilometers from the source fault.

7. Conclusion

We first studied the influence of different catalog intervals on seismicity around the six major strike-slip faults in southwest Japan studied by Stirling *et al.* We found no essential difference between the two catalog intervals with the exception of the Tanna fault, where the characteristic earthquake, i.e., the Kita-Izu earthquake ($M=7.3$), occurred in 1930. Then, we used new information on the Quaternary active faults obtained by HERP and a new algorithm to extract seismicity around the fault. A comparison of the occurrence rate of maximum-sized earthquakes estimated from geological information with instru-

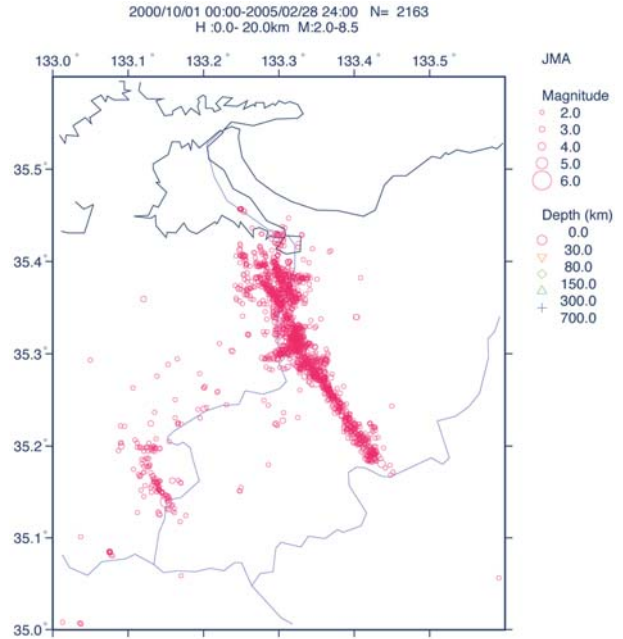


Fig. 9. Epicenter distribution of source region for the 2000 Western Tottori earthquake ($M=7.3$) with magnitudes 2.0 and above. Catalog interval is from October 2000 to February 2005 (from seismicity analysis system on WWW; Tsuruoka, 1997).

mentally recorded small and moderate earthquakes around the 24 segmented active faults or fault zones indicates that the number of observed events is significantly less than the number of events predicted by the G-R relationship for almost all faults or fault systems. The frequency ratio of the number of observed events to that predicted by the G-R relationship is about 0.10 (10%) on average. Therefore, the remaining 0.90 (90%) have to be filled by aftershocks or some anomalously high episodic seismicity if the G-R relationship holds during one earthquake cycle. However, an analysis of the 1930 Kita-Izu earthquake ($M=7.3$) shows that the number of aftershocks is too small to account for the absence. Although the regional seismicity is described well by the G-R relationship, the magnitude frequency distribution for individual source regions is rather close to the Characteristic Earthquake Model.

Acknowledgements

We thank the anonymous referee who gave useful comments and suggestions. To extract the aftershock sequence accompanying the 2000 Western Tottori Earthquake, we used the seismicity analysis sys-

tem on WWW of Dr. H. Tsuruoka (Tsuruoka, 1997) and thank him.

In this study, we used the unified Japan Meteorology Agency (JMA) catalog, which is compiled from data of Hokkaido University, Hirosaki University, Tohoku University, Tokyo University, Nagoya University, Kyoto University, Kochi University, Kyushu University, Kagoshima University, Shizuoka Prefecture, Yokohama City, Tokyo Metropolis, JMA, Natural Research Institute for Earth Science and Disaster Prevention, National Institute of Advanced Industrial Science and Technology (AIST), Japan Agency for Marine-Earth Science and Technology (JAMSTEC), and Hot Springs Research Institute of Kanagawa Prefecture. We thank these institutes.

References

- Aki, K., 1965, Maximum likelihood estimates of b in the formula $\log N = a - bM$ and its confidence limits, *Bull. Earthquake Res. Inst.* **43**, 237–239.
- Aki, K. and P.G. Richards, 1980, *Quantitative Seismology: Theory and Methods*, W. H. Freeman, San Francisco, California, 1–932.
- Bender, B., 1983, Maximum likelihood estimation of b -values for magnitude grouped data, *Bull. Seism. Soc. Am.*, **73**, 831–851.
- Earthquake Research Committee, 2003a, Long-term evaluation of the Yamasaki fault system, 38pp.
- Earthquake Research Committee, 2003b, Long-term evaluation of the Median Tectonic Line, 71pp.
- Earthquake Research Committee, 2004a, Long-term evaluation of the Atotsugawa fault system, 28pp.
- Earthquake Research Committee, 2004b, Long-term evaluation of the Atera fault system, 48pp.
- Earthquake Research Committee, 2005a, Long-term evaluation of the Kita-Izu fault system, 28pp.
- Earthquake Research Committee, 2005b, Long-term evaluation of the Nobi fault system, 49pp.
- Frohlich, C. and S. Davis, 1993, Teleseismic b -values: or, much ado about 1.0, *J. Geophys. Res.* **98**, 631–644.
- Gutenberg, B. and C.F. Richter, 1944, Frequency of earthquakes in California, *Bull. Seism. Soc. Am.* **34**, 185–188.
- Hamilton R.M., 1967, Mean magnitude of an earthquake sequence, *Bull. Seism. Soc. Am.*, **134**, 1115–1116.
- Hanks, T. and H. Kanamori, 1979, A moment magnitude scale, *J. Geophys. Res.* **84**, 2348–2350.
- Ishimoto, M. and K. Iida, 1939, Observations sur les seisms enregistre par le micorseismograph construite dernierment (I), *Bull. Earthquake Res. Inst. Univ. of Tokyo* **17**, 443–478.
- Itaba, S., K. Watanabe, R. Nishida and T. Noguchi, 2004, Quantitative evaluation of inland seismicity, *Monthly gogai-chikyū*, **46**, 146–153 (in Japanese).
- Japan Seismic Hazard Information Station (J-SHIS). <http://www.j-shis.bosai.go.jp/>
- Matsuda, T., 1975, Magnitude and recurrence interval of earthquakes from fault, *J. Seis. Soc. Jap. (Zisin)*, **28**, 269–283 (in Japanese with English abstract)
- Mogi, K., 1985, “Earthquake Prediction.” *Academic Press*, New York, 355p.
- Obara, K., K. Kasahara, S. Hori and Y. Okada, 2005, A densely distributed high-sensitivity seismograph network in Japan: Hi-net by National Research Institute for Earth Science and Disaster Prevention, *Rev. Sci. Instrum.* **76**, 021301.
- Page, R., 1968, Aftershocks and microaftershocks of the great Alaska Earthquake of 1964, *Bull. Seism. Soc. Am.*, **58**, 1131–1168.
- Papadopoulos, G., Skafida, H. and Vassiliou, I., 1993, Nonlinearity of the magnitude-frequency relation in the Hellenic Arc-Trench system and the characteristic earthquake model. *J. Geophys. Res.*, **98**, 0148–0227.
- Papadopoulos, G., Karastathis, V., Ganas, A., Pavlides, S., Fokaefs, A. and Orfanogiannaki, K., 2003, The Lefkada, Ionian Sea (Greece), shock (Mw 6.2) of 14 August 2003: evidence for the Characteristic Earthquake from seismicity and ground failures. *Earth, Planets and Space*, **55**, 713–718.
- Research Group for Active faults of Japan, 1980, *Map of active faults in Japan with an explanatory text*, Univ. of Tokyo Press, Tokyo.
- Research Group for Active faults of Japan, 1991, *Map of active faults in Japan with an explanatory text, revised edition*, Univ. of Tokyo Press, Tokyo.
- Schwartz, D.P. and K.J. Coppersmith, 1984, Fault behavior and characteristic earthquakes: examples from Wasatch and San Andreas fault zones, *J. Geophys. Res.*, **89**, 5681–5698.
- Shi, Y. and B.A. Bolt, 1982, The standard error of the magnitude-frequency b -value, *Bull. Seism. Soc. Am.*, **72**, 1677–1687.
- Shimazaki, K., 1986, Small and large earthquakes: The effect of thickness of seismogenic layer and the free surface. In Das, S., Boatwright, J. and Scholz, C. H. eds.: *Earthquake source mechanics*. AGU, Washington, D.C., 209–216.
- Sieh, K.E., 1981, A review of geological evidence for recurrence times of large earthquakes. In Simpson, D.W. and Richards, P.G. eds. *Earthquake Prediction, an international review*. Maurice Ewing Ser., 4. AGU, Washington, D.C., 181–207.
- Somerville, P., K., Irikura, R. Graves, S. Sawada, D. Wald, N. Abrahamson, Y. Iwasaki, T. Kagawa, N. Smith, A. Kowada, 1999, Characterizing crustal earthquake slip models for the prediction of strong ground motion, *Seismological Research Letters*, **70**, 59–80.
- Stirling, M.W., Wesnousky, S.G. and K. Shimazaki, 1996, Fault trace complexity, cumulative slip, and the shape of the magnitude frequency distribution for strike-slip faults: a global survey, *Geophys. J. Int.*, **124**, 833–868.
- Takemura, M, T. Ikeura, R. Sato, 1990, Scaling relations for source parameters and magnitude of earthquakes in the Izu peninsula region, Japan, *Tohoku Geophys. Journ.* **32**, 77–89.
- Takemura, M., 1990, Magnitude-seismic moment relations for the shallow earthquakes in and around Japan, *Zishin* **2**, **43**, 257–265.

- Takemura, M., 1998, Scaling law for Japanese intraplate earthquakes in special relations to the surface faults and the damages, *Zishin-2*, **51**, 211-228.
- The Headquarters for Earthquake Research Promotion. <http://www.jishin.go.jp/main/index.html>
- Tsuruoka, H., 1997, Development of seismicity analysis system on WWW (2), Programme and Abstracts, The Seismological Society of Japan, P04.
- Utsu, T., 1965, A method for determining the value of b in a formula $\log n = a - bM$ showing the magnitude frequency relation for earthquakes, *Geophys. Bull. Hokkaido. University*, **13**, 99-103 (in Japanese).
- Wallace, R.E., 1970, Earthquake recurrence intervals on the San Andreas Fault, *Geol. Soc. Am. Bull.*, **81**, 2875-2890.
- Wells, D.L., Coppersmith K.J., 1994, New empirical relationships among magnitude, rupture length, rupture width, rupture area, and surface displacement, *Bull. Seism. Soc. Am.*, **84**, 974-1002.
- Wesnousky, S.G., C.H. Scholz, K. Shimazaki and T. Matsuda, 1983, Earthquake frequency distribution and the mechanics of faulting, *J. Geophys. Res.*, **88**, 9331-9340.
- Wesnousky, S.G., 1986, Earthquakes, Quaternary faults, and seismic hazard in California, *J. Geophys. Res.* **91**, 12587-12631.
- Wesnousky, S.G., 1994, The Gutenberg-Richter or Characteristic Earthquake distribution, which is it ?, *Bull. Seism. Soc. Am.*, **84**, 1940-1959.
- Youngs, R. and K. Coppersmith, 1985, Implications of fault slip rates and earthquake recurrence models to probabilistic hazard estimates, *Bull. Seism. Soc. Am.*, **75**, 939-964.

(Received October 15, 2007)

(Accepted February 21, 2008)

Appendix A: Empirical relationship between seismic moment of maximum-sized earthquake and fault length

We used the empirical relationship between seismic moment of maximum-sized earthquake and fault length proposed by Wesnousky *et al.* (1983). However, various empirical relationships have been proposed. Here, we introduce four empirical relationships between seismic moment and fault length to examine the extent to which differences among them are recognized, will show that these differences are all contained within the bounding estimates used in this study.

Matsuda (1975) proposed an empirical relationship between magnitude of characteristic event and fault length using 14 inland earthquakes in Japan ranging from the 1891 Nobi earthquake to the 1970 Southeastern Akita earthquake and obtained the relationship below.

$$\log L = 0.6M - 2.9 \quad (6 \text{ again}),$$

The magnitude-fault dimension relationship together with the magnitude - displacement relationship for historical inland earthquakes in Japan from Matsuda (1975) are displayed in Figure A-1. HERP adopted this relationship to estimate the magnitude of maximum-sized earthquake from mapped fault length. On the other hand, Takemura *et al.* (1990) discussed the relationship between seismic moment and JMA magnitude from seismicity around the Izu peninsula, and obtained the empirical relationship

below.

$$\log M_0 = 1.17M_{JMA} + 17.72 \quad (\text{in unit of } \text{dyne} \cdot \text{cm}) \quad (\text{A-1})$$

where M_0 is seismic moment, and M_{JMA} is JMA magnitude. Takemura (1990) insists that this empirical relationship can be applied to general inland shallow earthquakes including the 1891 Nobi earthquake. By combining equation (6) and equation (A-1), the relationship between seismic moment (in unit of $\text{dyne} \cdot \text{cm}$) and fault length (in unit of kilometer) is obtained.

$$\log M_0 = 1.95 \log L + 23.375 \quad (\text{A-2})$$

Shimazaki (1986) collected fault parameters for 25 earthquakes (22 crustal earthquakes and 3 earthquakes that occurred in the eastern margin of the Japan Sea; the 1940 Shakotan-Oki earthquake, the 1964 Niigata earthquake and the 1983 Nihon-Kai-Chubu earthquake), and proposed the following empirical relationship between seismic moment and fault length.

$$\log L = 0.281 \log M_0 - 5.98 \quad \text{for} \quad M_0 \leq 7.5 \times 10^{25} \text{ dyne} \cdot \text{cm} \quad (\text{A-3})$$

$$\log L = 0.524 \log M_0 - 12.44 \quad \text{for} \quad M_0 \geq 7.5 \times 10^{25} \text{ dyne} \cdot \text{cm} \quad (\text{A-4})$$

where $7.5 \times 10^{25} \text{ dyne} \cdot \text{cm}$ is the seismic moment corresponding to a fault width saturated by the thickness of the seismogenic layer. He pointed out that the scaling law changes from $M_0 \propto L^3$ to $M_0 \propto L^2$ at this seismic moment. Moreover, he thought the disconti-

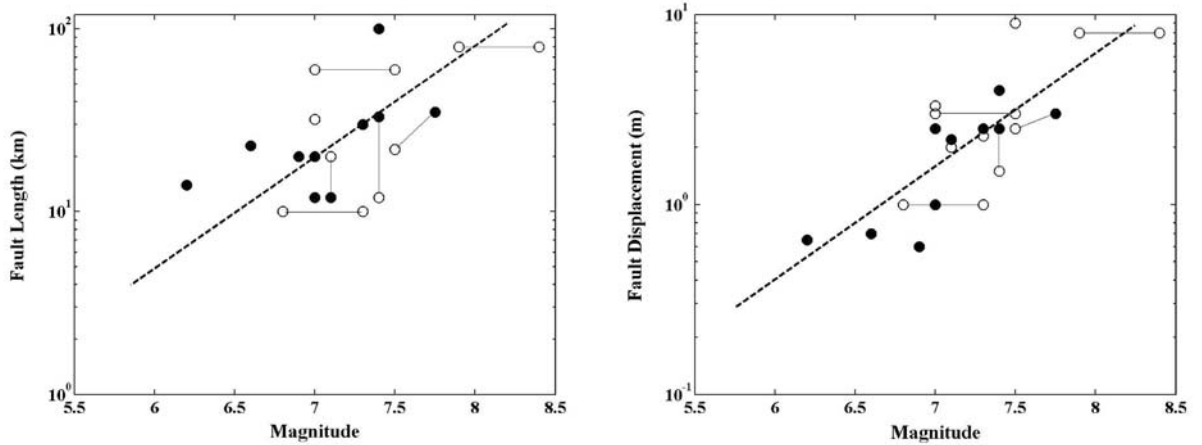


Fig. A-1. Magnitude-fault dimension relation and magnitude-displacement relation of historic earthquakes in inland Japan from Matsuda (1975). Open circles represent observed values on the surface and filled black circles represent values from seismological or geodetic data.

nunity at seismic moment $7.5 \times 10^{25} \text{ dyne*cm}$ is caused by events with seismic moments greater than $7.5 \times 10^{25} \text{ dyne*cm}$ that accompany surface rupturing. Takemura (1998) obtained a new relationship based on this scaling law and obtained

$$\log L = \frac{1}{3} \log M_0 - 7.28 \quad \text{for} \quad M_0 \leq 7.5 \times 10^{25} \text{ dyne*cm} \quad (\text{A-5})$$

$$\log L = \frac{1}{2} \log M_0 - 11.82 \quad \text{for} \quad M_0 \geq 7.5 \times 10^{25} \text{ dyne*cm} \quad (\text{A-6})$$

Wells and Coppersmith (1994) compiled fault parameters, and obtained the empirical relation between moment magnitude and surface rupture length described in equation A-7.

$$M_w = 1.16 \log L + 5.108 \quad (\text{A-7})$$

Using the definition of moment magnitude, we can also convert this equation into the relationship between seismic moment and surface rupture length.

$$\log M_0 = 15 M_w + 16.1 \quad (16 \text{ again})$$

$$\log M_0 = 1.74 \log L + 23.72 \quad (\text{A-8})$$

where, M_w is moment magnitude. Figure A-2 shows the various proposed empirical equations. Figure A-3 shows estimated seismic moment based on fault length using the empirical relationships. Figure A-3 indicates that the various empirical relationships are all contained within the bounding estimates used in this study where the fault length is greater than 20 kilometers. Faults covered in this study are fundamentally longer than 20 kilometers, therefore, changes to the scaling law proposed by Shimazaki (1986) and Takemura (1998) can be neglected.

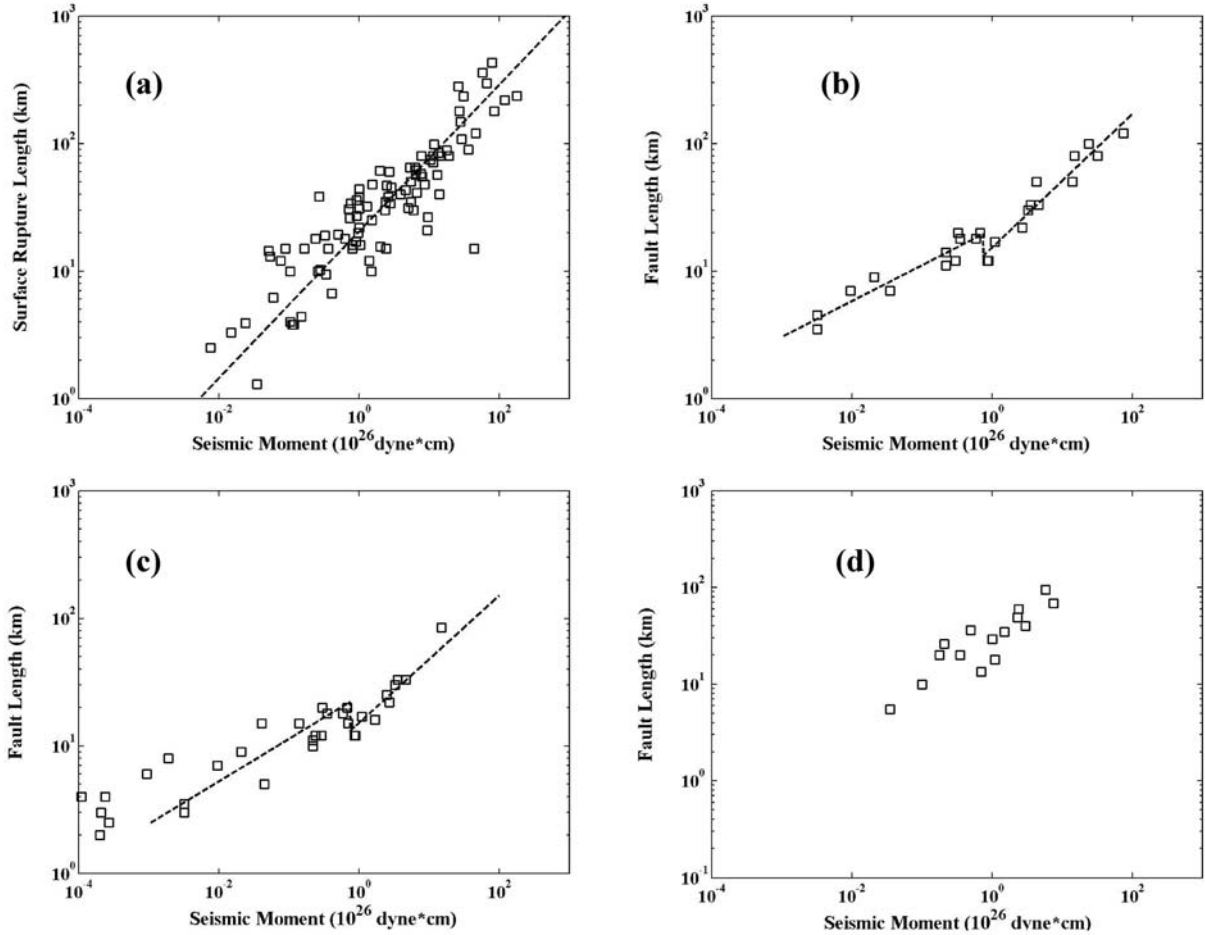


Fig. A-2. Various empirical relationships between seismic moment and fault length. (a) Relationship between moment magnitude and surface rupture length from Wells and Coppersmith (1994) is converted into relationship between seismic moment and surface rupture length using the definition of moment magnitude from Hanks and Kanamori (1979). (b), (c), and (d) are relationships between seismic moment and fault length from Shimazaki (1986), Takemura (1998), and Somerville *et al.* (1999), respectively.

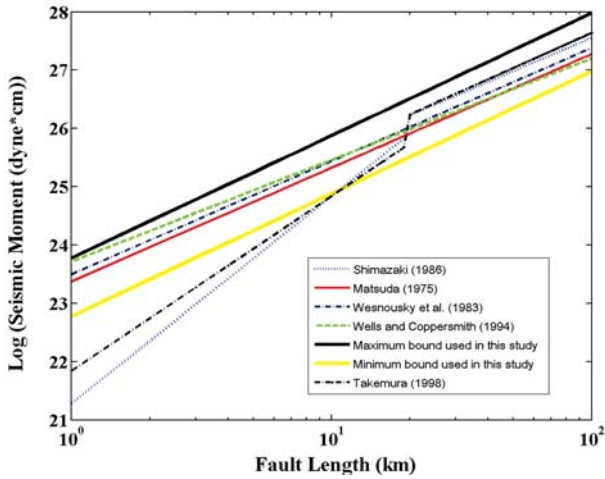


Fig. A-3. Empirical relationships between fault length and seismic moment. Matsuda (1975), Wesnousky *et al.* (1983), Shimazaki (1986), Wells and Coppersmith (1994) and Takemura (1998) are indicated together with the minimum and maximum bounds in this study.

Appendix B: Fault Segmentation for the six strike slip fault systems estimated by HERP

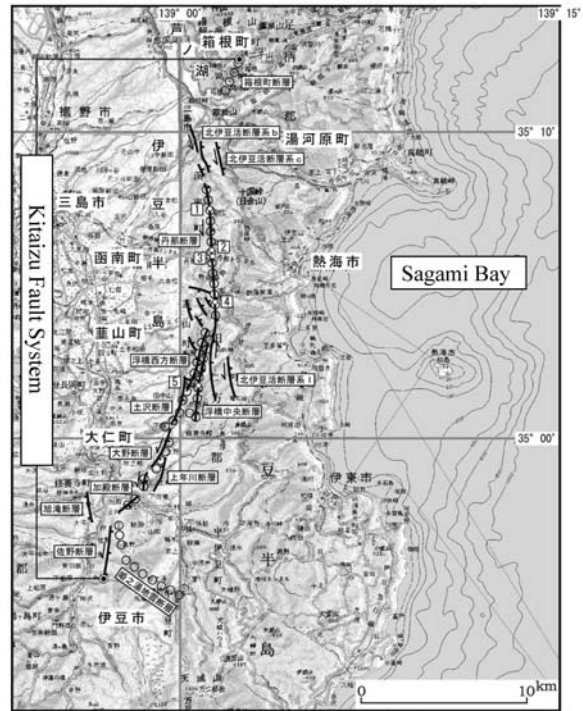


Fig. B-1. Fault trace of the Kita-izu fault system modified from Earthquake Research Committee (2005a). Open circles indicate the surface rupture fault accompanying the 1930 Kita-Izu earthquake.

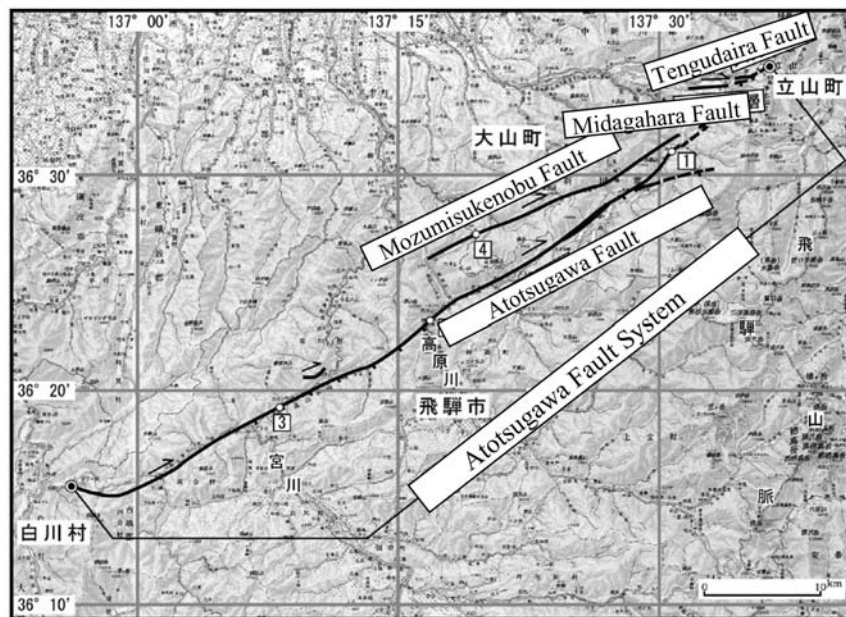


Fig. B-2. Fault trace of the Atotsugawa fault system modified from Earthquake Research Committee (2004a).

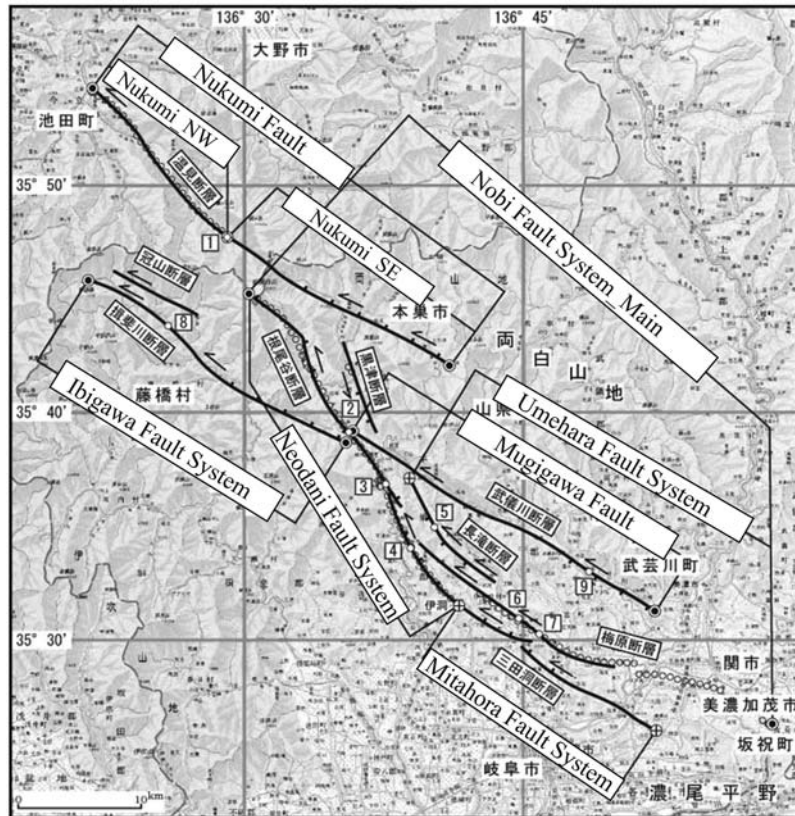


Fig. B-3. Fault trace and fault segmentation of the Nobi fault system modified from Earthquake Research Committee (2005b). The open circles indicate the surface rupture fault accompanying the 1891 Nobi earthquake.

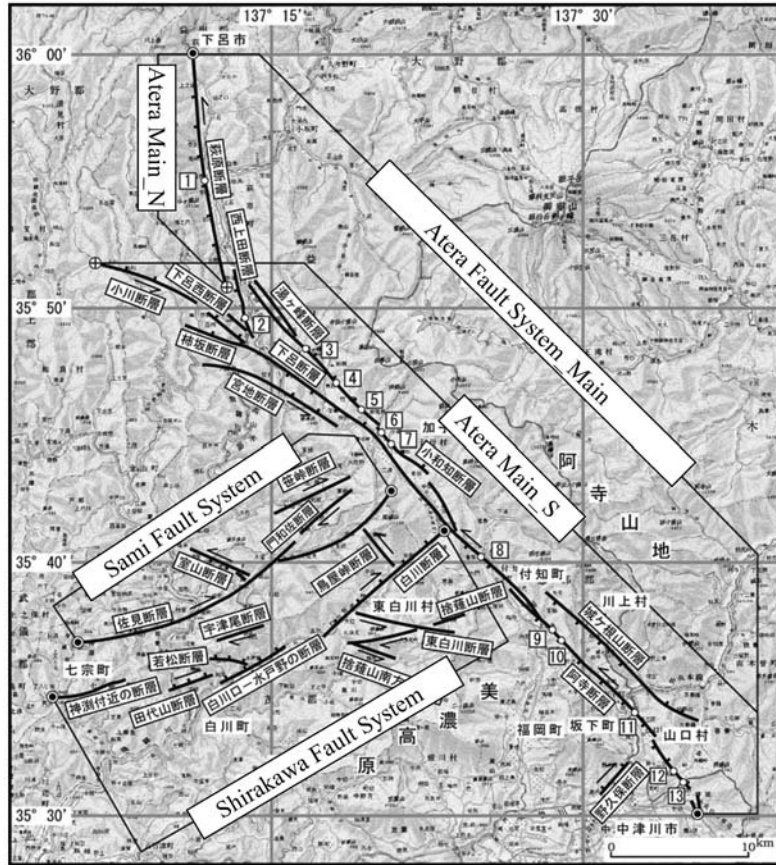


Fig. B-4. Fault trace and fault segmentation of the Atera fault system modified from Earthquake Research Committee (2004b).

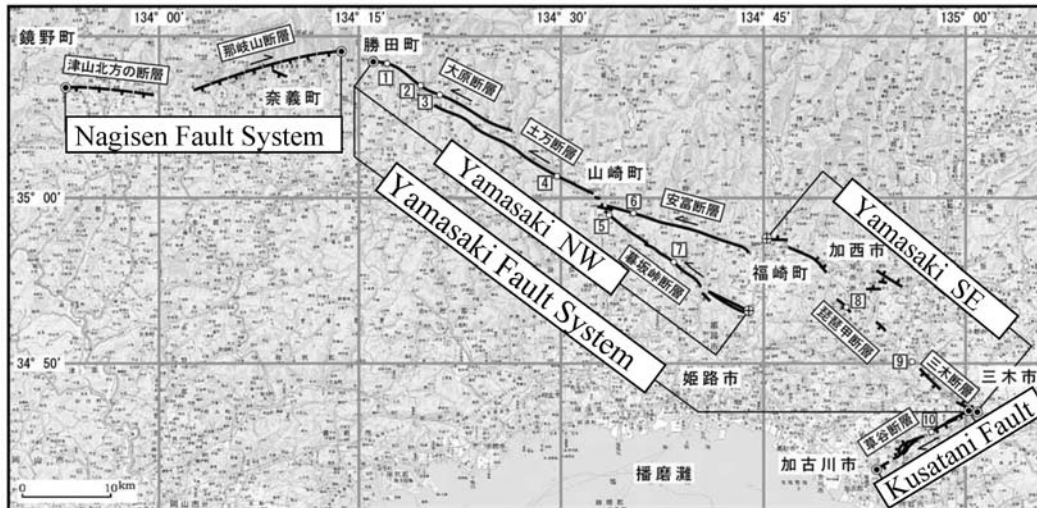


Fig. B-5. Fault trace and fault segmentation of the Yamasaki fault system modified from Earthquake Research Committee (2003a).

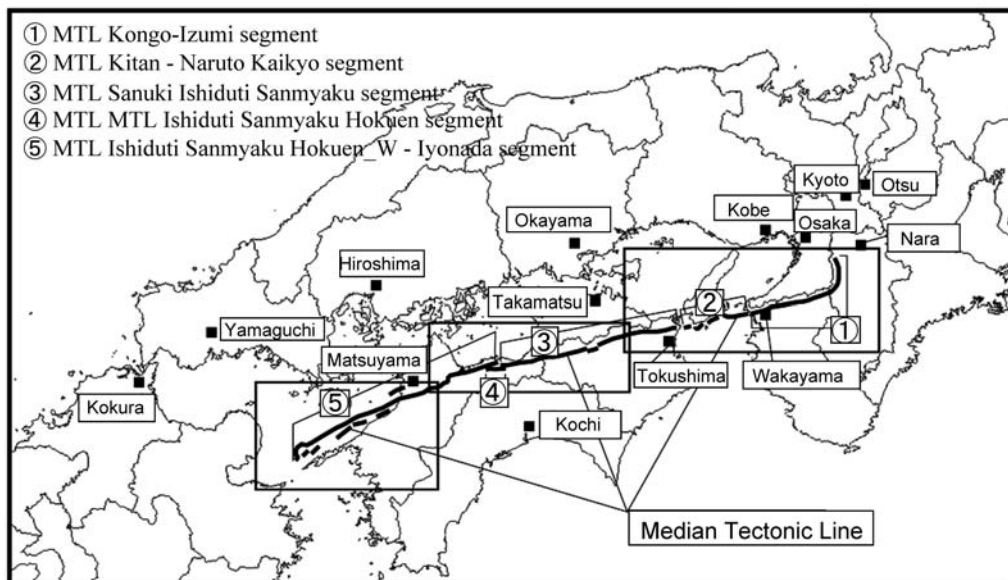


Fig. B-6. Fault trace and fault segmentation of the Median Tectonic Line modified from Earthquake Research Committee (2003b).